According to the Wiener-Khinchine theorem, the spectral density $S(\omega)$ is the Fourier transform of the autocorrelation function, and therefore

$$R_f(r) = \int_{-\infty}^{\infty} e^{i\omega r} S(\omega) d\omega = \int_{-\infty}^{\infty} \cos(\omega r) S(\omega) d\omega. \tag{2.67}$$

Substituting 2.67 in 2.66, we find

$$\begin{aligned} D_f(r) &= -2R_f(r) + D_f(\infty) = -2R_f(r) + 2R_f(0) & (2.68)\\ &= 2\int_{-\infty}^{\infty} (1 - \cos \omega r) S(\omega) d\omega. & (2.69) \end{aligned}$$

For a spectral density function $S(\omega) = A|\omega|^{-(p+1)}$, with $A > 0$, and $0 < p < 2$, we find the structure function using 2.68:

$$\begin{aligned} D_f(r) &= 2A \int_{-\infty}^{\infty} (1 - \cos \omega r) |\omega|^{-(p+1)} d\omega & (2.70)\\ &= \frac{2A\pi}{\sin \frac{\pi p}{2} \Gamma(1+p)} r^p. & (2.71) \end{aligned}$$

In other words, the structure function $D_f(r) = c^2 r^p$, with $0 < p < 2$, corresponds to the spectral density function

$$S(\omega) = \frac{\Gamma(1+p)}{2\pi} \sin \frac{\pi p}{2} c^2 |\omega|^{-(p+1)} \tag{2.72}$$

An observed spectral density with a $-5/3$ power law will therefore correspond to a structure function $D_f(r) = c^2 r^{2/3}$.

2.4.6 Ionospheric influence

Using equation (2.39), step 2 of the model yields

$$\frac{\partial \psi_1(x,y)}{\partial x} = \frac{4\pi}{\lambda \cos\theta} \frac{-40.28}{f^2} \frac{\partial TEC(x,y,t_1)}{\partial x}. \tag{2.73}$$

Using TEC units of $10^{16}\mathrm{m}^2$, this is

$$\frac{\partial \psi_1(x,y)}{\partial x} = -0.55 \frac{\partial TEC(x,y,t_1)}{\partial x} \cdot 2\pi. \tag{2.74}$$

This means that a horizontal change of 1 TECU over one SAR scene results in a phase ramp of -0.55 cycle. In the interferometric phase, step 3, the difference of two phase observations is taken, hereby largely eliminating daily variation. Note that the sign of the factor is negative, i.e. an increase in TEC results in a phase advance.

Following equation (2.74), if ionospheric effects have an observable influence in a single SAR scene, the dominant wavelength should be less than 100 km, to distinguish them from orbit errors, while the amplitude should be more than 0.36 TEC, to get a signal of 0.2 phase cycles.

The only natural phenomena that could possibly cause such effects are small scale Traveling Ionospheric Disturbances (TIDs), with a wavelength of tens of km (Spoelstra, 1997). These TIDs are wave effects, mostly propagating from polar regions to regions with lower latitudes.

2.4.7 Distinguishing between ionospheric and tropospheric effects

The difference between ionospheric and tropospheric effects on SAR interferometry is based on two characteristics: the sign of the delay and the shape of the feature. From equation 2.39, it follows that increase in the ionospheric electron content results in a decrease of the observed range, or a *phase advance*. An area of increased partial water vapor pressure, see equation 2.28, results in an increase in the observed range, or a *phase delay*. However, there are two complications:

1. one has to know during which of the two SAR images the effect occurred: a phase *advance* in the first image gives the same result as a phase *delay* in the second one, and

2. one has to distinguish which area in the interferogram can be regarded as reference area, where the phase is relatively undisturbed: a localized area with *reduced* water vapor density yields a localized relative *advance* of the phase.

The first complication can be solved only when using more than two SAR images. The different interferometric combinations of images enables the unambiguous identification of the image containing the errors, as long as other error sources such as temporal decorrelation allow for such an evaluation. Since for this study only single interferometric pairs were used, it is not possible to distinguish between phase delay and advance based on only interferometric data.

The second complication, however, is much harder to circumvent. Just as localized areas with an increased water vapor content occur frequently, in a relative sense also areas with a lesser amount of water vapor occur. This can be clearly observed in, e.g., Meteosat water vapor channel imagery. Therefore, without any additional information it is not possible to uniquely identify ionospheric effects in interferograms based on the phase sign of the feature.

The remaining possibility for identification is based on the shape and characteristics of the feature. The main difficulty in this respect is the limited knowledge about the spatial characteristics of the ionosphere within ranges of less than 100 km. Although different devices using dual-frequencies have observed the ionosphere, their results have either been only one-dimensional integrated profiles (as is, e.g., possible with GPS), or large scale interpolated ionospheric maps, which do not have the spatial resolution needed for InSAR.

Based on these evaluations, it is difficult to uniquely identify ionospheric effects in SAR interferograms at present, unless strong support from additional sources is available. It should be noted however, that further research in this field, using, e.g., dual frequency SAR interferometry, could be extremely valuable for its ionospheric imaging capacities.

Chapter 3

Interferometric Database

This chapter describes the interferometric database analyzed in this study. The choice of suitable test sites is discussed using a set of selection criteria, and the coding conventions used in chapter 5 are listed. The second section briefly describes the used procedure in the interferometric processing and the post processing, such as a posteriori multilooking, extraction of the reference elevation model, orbit errors, and masking.
key words: interferometric processing, selection criteria, DEM

3.1 Test site locations

The repeat pass interferometric phase can be considered as a juxtaposition of several physical signals, such as topography, deformation in slant range direction, propagation delays, orbital configuration, surface penetration, changes in the dielectric properties of the surface, and noise due to different kinds of decorrelation. In order to investigate one specific signal one has to carefully remove the influence of all the others.

For this study the main focus is on the influence of atmospheric effects or propagation delay differences. In order to eliminate or minimize the effects of other signals, test sites were chosen with near optimal conditions. Since topography in the Netherlands is limited and very well known, test sites in this area are either free of topographic phase or it can be easily corrected for. In order to minimize the effect of temporal decorrelation and possible deformations between the image acquisitions, ERS tandem imagery was used only. More than one test site was chosen, in order to analyze an amount of interferograms which is enough to cover a full seasonal cycle. The use of different test sites also provides possibilities to discern between coastal and more inland areas. Interferometric phase changes due to the orbital configuration were minimized using precise a posteriori orbit information.

Now, the remaining interferometric phase consists of atmospheric propagation heterogeneities and surface interaction. It is observed that phase signatures due to surface interaction are mostly of limited spatial extent, and often strongly correlated with differences in land use, which can be detected in the SAR backscatter imagery. Therefore, for the majority of interferometric phase signal, it can be concluded that only the atmosphere is being observed.

Figure 3.1 shows the location of the test sites and SAR frames. The frames are coded as described in table 3.1. The dots at the map indicate the positions of the meteorological

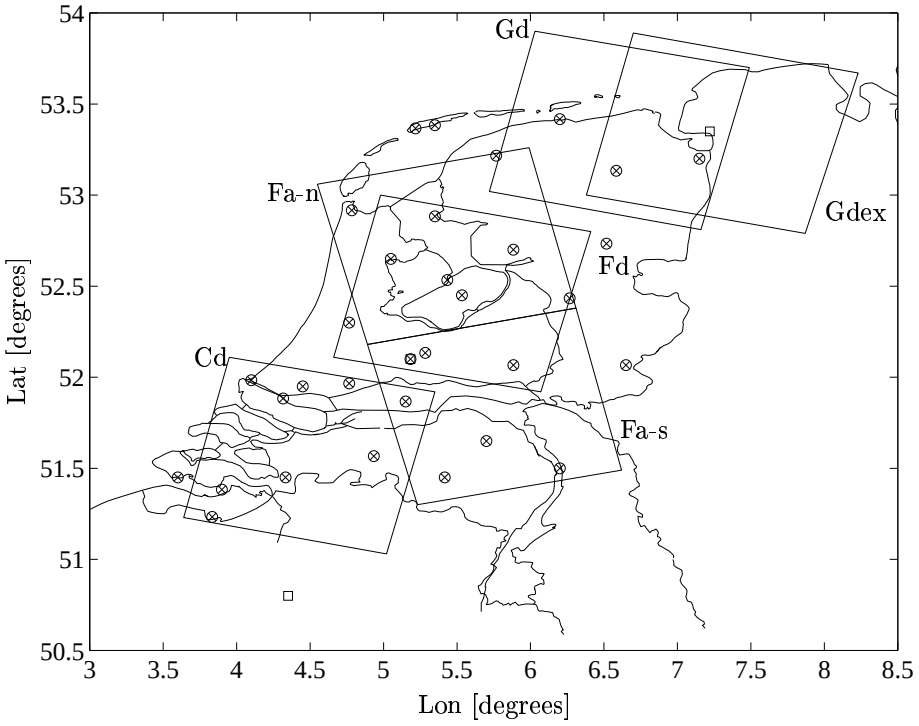

Figure 3.1 *Location of the test sites, SAR acquisitions and meteorological stations. The circles indicate synoptic stations, the squares are radiosonde locations.*

stations, whose information was used in the interpretation of the interferograms. The large amount of available meteorological observations was in fact another reason for this particular choice of test locations in the Netherlands.

Code	Full name
gd	Groningen descending
gdex	Groningen descending, adjacent track
fd	Flevoland descending
fa-n	Flevoland ascending north
fa-s	Flevoland ascending south
cd	CLARA (Delft) descending

Table 3.1 *Codes used for the different test sites. The CLARA interferogram was acquired during the CLouds And RAdiation meteorological experiment.*

3.1.1 List of interferograms

The 26 interferograms analyzed in this study are categorized according to their location. The database with SAR-SLC input data, and interferometric combination, is listed in table 3.2. The list shows the identification code, dates of acquisition, orbit number, the SAR processing and archiving facility, and the estimates for the parallel baseline and the perpendicular baseline. Track and frame numbers are shown at the top of each location. The position of the interferograms is shown in figure 3.1.

No.	ID	Date	ERS-1	PAF	ERS-2	PAF	$B^{\parallel}$	$B^{\perp}$
		Groningen descending, track 380 frame 2529						
1	Gd-1	15/16-07-95	20909	D	1236	I	3	-27
2	Gd-2	19/20-08-95	21410	D	1737	D	37	81
3	Gd-3	02/03-12-95	22913	D	3240	D	17	44
4	Gd-4	16/17-03-96	24416	I	4743	I	16	-18
5	Gd-5	20/21-04-96	24917	D	5244	D	34	67
6	Gd-6	25/26-05-96	25418	I	5745	I	52	99
7	Gd-7	03/04-08-96	26420	UK	6747	I	46	103
		Flevoland descending, track 151 frame 2547						
8	Fd-1	03/04-08-95	21181	D	1508	D	32	58
9	Fd-2	07/08-09-95	21682	D	2009	D	30	37
10	Fd-3	12/13-10-95	22183	D	2510	D	-127	-324
11	Fd-4	16/17-11-95	22684	D	3011	D	259	531
12	Fd-5	21/22-12-95	23185	D	3512	D	62	173
13	Fd-6	04/05-04-96	24688	I	5015	D	26	59
14	Fd-7	13/14-06-96	25690	UK	6017	D	45	77
		Flevoland ascending south, track 29 frame 1035						
15	Fa-s1	29/30-08-95	21560	D	1887	D	-31	-80
16	Fa-s2	03/04-10-95	22061	D	2388	D	146	393
17	Fa-s3	26/27-03-96	24566	D	4893	D	-21	-33
18	Fa-s4	30-04/01-05-96	25067	UK	5394	UK	-31	-59
19	Fa-s5	04/05-06-96	25568	UK	5895	I	-35	-89
		Flevoland ascending north, rack 29 frame 1053						
20	Fa-n1	29/30-08-95	21560	D	1887	D	-30	-79
21	Fa-n2	03/04-10-95	22061	D	2388	D	144	385
22	Fa-n3	26/27-03-96	24566	D	4893	D	-21	-32
23	Fa-n4	30-04/01-05-96	25067	UK	5394	UK	-30	-57
24	Fa-n5	04/05-06-96	25568	UK	5895	I	-34	-88
		CLARA (Delft) descending, track 423 frame 2565						
25	Cd-1	23/24-04-96	24960	UK	5287	UK	38	78
		Groningen adjacent descending, track 108 frame 2529						
26	Gdex-2	26/27-02-96	24144	D	4471	D	-15	-31

Table 3.2 *A listing of the interferograms of this study. The interferograms have been coded, in the second column. The fourth and sixth column give the orbit numbers for ERS-1 and ERS-2 respectively, the fifth and seventh column indicate the Processing and Archiving Facility, responsible for the SAR-SLC processing (**D**: German, **I**: Italian, and **UK**: the United Kingdom). The last two columns give an estimation for the parallel baseline and the perpendicular baseline in meters.*

3.2 Processing of the interferograms

The interferometric processing was performed using DLRs GENESIS system (Schwäbisch and Geudtner, 1995; Schwäbisch, 1995; Eineder and Adam, 1997). First, the two full single look complex (SLC) ERS SAR images are coregistered and the corresponding regions are determined. Spectral filtering is applied to reduce the effect of baseline induced noise. After fast resampling of the second image, complex multiplication is performed to obtain the phase interferogram. Precise orbit information was used from DLR-GFZ and in some cases DEOS. Based on the orbit state vectors, a reference interferogram based on the WGS84 ellipsoid is subtracted, which yields the "flattened" interferogram.

In first instance, a multilook level corresponding to 2 resolution cells in range, and 10 in azimuth direction was chosen. Coherence images were calculated and used for further analysis. Phase unwrapping was performed using either the minimal cost flow (Costantini, 1996) algorithm implementation at DFD-DLR, or the method of Ghiglia and Romero (1994). The first method resulted in an almost perfect unwrapped interferogram, although some areas which were isolated by water had 2π jumps. These, however, were easily recognized and mostly corrected for afterward. The second method did not have the 2π jumps (except for some islands), but had a limited amount of unwrapping "pits" caused by unconnected residues. When necessary, these pits were corrected for manually.

3.2.1 A posteriori multilook

To reduce data size and facilitate storage capacities, the interferograms are subsampled by a factor 4 in range and azimuth direction. The pixels in the images now roughly correspond to a ground area of 160×160 meters. Since it is expected that atmospheric signal below this pixel size is not strong enough to be distinguished in the interferograms, this appeared to be a practically useful choice.

3.2.2 Reference elevation model

The standard elevation model *TopHoogteMD* (Topografische Dienst Nederland and Meetkundige Dienst Rijkswaterstaat, 1997) was used to correct for the topographically induced phase variation. This was necessary only for those situations which had significant topography in combination with a rather large baseline. The TopHoogteMD DEM consists of heights with respect to the local NAP[1] reference surface, which are close to orthometric heights with respect to the geoid. The used coordinate system is the local RD[2] system, which is transformed to WGS84 coordinates for this study.

Depending on the analysis, two methods were followed. In the first, the orbit information of the spacecraft was used to calculate a synthetic interferogram from the reference DEM. This synthetic interferogram was compared with the observed interferogram, and registered using a maximum correlation method. Subtraction of the synthetic interferogram from the observed interferogram yielded the differential interferogram. The differential interferogram is still in the slant-range azimuth coordinate system, but reveals no more topographic phase variation. In the second method, the observed interferogram was geocoded to the WGS84 latitude-longitude system. In this reference system, the reference

[1] Normaal Amsterdams Peil
[2] Rijksdriehoeksmeting

DEM can be easily subtracted, yielding a geocoded differential interferogram.

After the elimination of the topographic phase, only differential signal remains in the interferograms. Since the time interval between the SAR acquisitions was only 24 hours, it is not expected that significant deformations occurred in between, and therefore the only phase signal should be of atmospheric nature.

3.2.3 Orbit errors

The orbit accuracy of the used precise orbits is still not sufficient, and causes especially for small perpendicular baselines long wavelength disturbances in the interferograms. These disturbances are eliminated using the reference interferogram, and minimizing the overall error. Note that the use of tie-points in interferograms which have strong atmospheric artifacts can be a problem. Atmospheric phase gradients which are unaccounted for will result in tilts in the derived height model. Using a great number of tie-points will help minimizing this problem, although large scale atmospheric disturbances, e.g., those connected to frontal zones, will still cause remaining tilts.

3.2.4 Masking

Water areas and severely decorrelated areas (sometimes forests) are masked using coherence measures. For some interferograms, additional manual masking or de-masking is applied to optimize the interpretation of the phase information.

Chapter 4

Meteorological Database

This chapter briefly covers some important aspects of the meteorological information used for the interferogram analysis. In the first section, the different scales in atmospheric dynamics are briefly reviewed, followed by spatial and temporal scales in the observation networks used in this study. The second section gives an overview of the data sources and instrumentation used to interpret the series of interferograms in chapter 5. The two last sections provide some information on the feasibility of using contemporary meteorological models for the purpose of ERS SAR interferometry, and the code system used for automatic exchange of meteorological information.
key words: scales, observations, instrumentation, models, codification.

4.1 Scales

Both atmospheric phenomena and consequently observation networks cover a large bandwidth in spatial and temporal scales, reaching from microturbulence to global atmospheric phenomena, and from sub-seconds for microscale turbulent mixing to centuries for climatic change. The following sections describe the most important features of both atmospheric and observation scales. The subdivision in scale groups is important to assess which processes are influencing the spatial and temporal characteristics of SAR interferograms.

4.1.1 Scales in atmospheric phenomena

Much of the activity of the atmosphere can be arranged in a small number of temporal and spatial scales. Table 4.1, adjusted from McIlveen (1995), lists a number of weather-related atmospheric disturbances with its respective scale characteristics. The bold-faced part of the table represents the phenomena which can be observed using tandem ERS SAR interferometry.

Convection ranges from small cumulus to big showers, *Mesoscale systems* consists of shower patterns, sea breezes, etc., *Synoptic scale systems* are extratropical and tropical cyclones etc., and *Hemispheric scale systems* are, e.g., long waves in tropospheric flow. Only the first three processes have spatial scales within the range of full scene range of ERS SAR interferograms.

spatial range [m]	Disturbance	temporal range [sec]
10^{-3}—10^{3}	**Turbulence**	10^{-1} — 10^{3}
10^{1}—10^{3}	**Convection**	10^{2} — 10^{4}
10^{3}—10^{5}	**Mesoscale systems**	10^{3} — 10^{5}
10^{5}—10^{7}	Synoptic scale systems	10^{4} — 10^{5}
$> 10^{7}$	Hemispheric scale	10^{6} — 10^{7}
$> 10^{7}$	Seasonal	10^{7} — 10^{9}
$> 10^{7}$	Climatic	$> 10^{9}$

Table 4.1 *Temporal and spatial scales in atmospheric dynamic processes (McIlveen (1995)). The bold faced disturbances are in the range of SAR interferometric observation.*

4.1.2 Observation scales

Like the different spatial and temporal scales in the atmospheric phenomena, the network of observations can also be developed into several scales (McIlveen, 1995). Actually, specific scales of atmospheric phenomena are referred to using observation network scales.

4.1.2.1 Surface network

The network of surface stations (operating manually or automatically) that are making *synoptic* (simultaneous) observations is also called the *synoptic network*. This synoptic network is able to define cyclones, anti-cyclones and their smaller scale frontal systems, which are therefore defined as *synoptic scale* weather phenomena. The synoptic scale network, however, fails to observe sub-synoptic scale systems such as shower clouds and the quite substantial clusters they sometimes form. Yet, the Netherlands can be regarded as a relatively well equipped country, with a number of 32 surface stations within an area of 200 $\times$ 300 km.

Regarding the temporal scales of the synoptic network, hourly observations of wind, temperature, humidity, pressure, visibility and cloud and weather types are made at each station of the network, just before the hour (in UTC). The precipitation totals, the manual gauge readings, are performed at 9:00 and 21:00 Local Time (LT), to reveal the systematic differences between day and night.

The weather radar network is also a part of the surface network. Weather radars can give a more specific overview of all substantial precipitation within range, although the field of view decreases with increasing range. The resolution is approximately 2 km at a distance of 100 km from the instrument.

4.1.2.2 Upper air network

Radiosondes provide observations of wind, temperature, relative humidity and pressure. From the De Bilt station, every 6 hours a sonde is released, which climbs with approximately 5 m/s to heights of 20–30 km. Temperature, humidity and pressure is sent by radio to the ground station, wind speed and direction are obtained by automatic tracking of the sonde by triangulation techniques.

4.1.2.3 Satellite network

Meteorological satellites make use of existing radiation emitted or reflected from the atmosphere. One or more wavelength bands are being observed by radiometers, usually in

the visible and infra-red range. Visible range imagery reveals the reflectance of sunlight on clouds. Therefore, it cannot be used at night. Infra-red sensing measures the terrestrial radiation emitted by the Earth's surface and atmosphere. The choice of the wavelength in the infra-red band determines the ease with which the clear air can be penetrated, and therefore, the elevation from which the emission originates. Horizontal resolutions for satellite imagery start from a few kilometers, and temporal sampling is dependent on the orbital configuration and the scanning rates of the instruments.

4.2 Data sources

This section describes the used data and instruments for the current study. The characteristics of the different instruments are summarized, and the resulting meteorological parameters are discussed.

4.2.1 Meteorological satellites

Satellite weather imagery provides different types of information. From observations in the visual channel, cloud types and coverage can be determined. Using infrared (IR) imagery, the heights of cloud tops can be studied, as well as temperature gradients between ocean and land. Water vapor imagery gives information on the integrated water vapor in the atmosphere. For all channels, a series of images provides information on wind speeds at different height levels. In this study, two spaceborne instruments are used: AVHRR and Meteosat.

4.2.1.1 AVHRR

The NOAA Advanced Very High Resolution Radiometer (AVHRR) has a spatial resolution of 1.1×1.1 km at nadir. It uses a whiskbroom scanner covering a ground swath of approximately 2000 km. The NOAA satellites are in a nearly polar, sun-synchronous orbit with a revolution time of approximately 100 minutes. The combination of two operational satellites with this wide ground swath allows a coverage of some 6–8 times per 24 hours. There are five channels:

- 0.58 – 0.68 micron,
- 0.73 – 1.1 micron,
- 3.6 – 3.9 micron,
- 10.3 – 11.3 micron, and
- 11.5 – 12.5 micron.

A combination of channels, assigning a different color to each channel, can help the visualization and interpretation of the data. For this study, a combination of channel 1, 2, and 4 is used. The cold cirrus clouds are shown in white, while the warmer medium and lower level clouds have more yellowish colors. AVHRR imagery can be used to get an overview of the general atmospheric situation, the position of frontal zones, and the type of cloud cover.

4.2.1.2 Meteosat

Meteosat imagery is obtained with a temporal sampling of 1 acquisition per half hour for each channel, according to a predefined scheme—e.g., no visual observations during nighttime—and with a spatial resolution of 5×5 km at nadir. For the latitude of the Netherlands, the spatial resolution is 5×9 km. Meteosat uses three channels:

- 0.5 - 0.9 micron (visual channel),
- 5.7 - 7.1 micron (water vapor channel), and
- 10.5 - 12.5 micron (infrared channel).

Meteosat is a geostationary satellite (35800 km height) located above the Greenwich meridian, and uses a spin scan radiometer to return images in the visible, infrared, as well as the water vapor band. The satellite records either the *normal visual*, *infrared* and *water vapor* combination, or only the so called *double visual* combination. The resolution at nadir is 5.0 km for infrared, water vapor, and normal visible, and 2.5 km for double visible. Due to the curvature of the Earth, the resolution along the meridian scales with $1/\cos(\varphi)$, where φ is the geocentric latitude. For the Netherlands, this means a resolution of about 5×8 kilometers in the first three modes, and 2.5×4 in the Double Visual mode. Therefore, it is not possible to discern small cumulus clouds. It is however, possible to get an overview of the weather situation, the location of fronts and depressions, etc. The higher temporal sampling, when compared to AVHRR, provides a better correlation with the ERS SAR acquisitions.

4.2.2 Weather radar

The weather radar data are a combination of the data acquired by two active radars: De Bilt and Schiphol. These radars use C-band microwave pulses and measure the scatter due to precipitation particles. The scatter intensity, azimuth direction and elevation angle of the radar, and time delay are combined into a scatter map, where the scatter intensity can be related to the precipitation rate in mm/hr. Such a scatter map is available every 15 minutes, and a series of scatter maps over some hours gives a clear insight in the progression and development of precipitation fields. The radar echos with highest elevation can be determined using the range and elevation. Corrections are applied for beam attenuation in rain, refraction, and side lobe echos.

By plotting the radar reflectivity against the rain rate, it has been found that it follows a power-law relationship: $Z = aR^b$, where Z is the radar reflectivity in units of ($\mathrm{mm}^6/\mathrm{m}^3$) and R is the rain rate in mm/hr. The relationship used by the KNMI radars is $Z = 200R^{1.6}$. The accuracy can often be a factor 3 too large or too small (Wessels, 1997). The beam width of the antenna is 1 degree, resulting in a linear decay in azimuth resolution moving away from the antenna.

Possible erroneous interpretation of the radar signal can be caused by the scattering of, e.g., inversion layers and high buildings. However, due to the characteristics of these signals, they can mostly be discerned from real precipitation. A further important feature of the radar is the lack of signal from the lowest levels of the atmosphere, which becomes dominant for precipitation far from the radar instrument, due to the Earth's curvature.

Therefore, it is possible that the radar senses precipitation up to hundred kilometer from the instrument, although this precipitation does not reach the ground, due to evaporation along its path.

4.2.3 Radiosonde

Radiosonde data (in meteorology also known as *TEMPs*) are acquired at a large number of meteorological stations in the world. Within the framework of the World Meteorological Organization (WMO), all observations are performed at the "synoptic" hours: 0, 6, 12, and 18 h UTC. The sonde performs the ascent in about one hour. At specified pressure levels a minimal set of observations is extracted and transfered to the national and international meteorological organizations.

The radiosonde system consists of an *instrument package*, a *radio receiver* a *tracking unit*, and a *recorder* (Hopkins, 1996). The instrument package contains a *thermistor*, which measures temperature with an accuracy of 0.2°C, a *hygristor*, which senses the relative humidity in the range from 15% to 100%, with an accuracy of 3.5%, and an *aneroid barometer* which measures pressure (Elliot and Gaffen, 1991). Apart from these meteorological instruments, it contains a radio transmitter and a battery. Wind speed and direction are obtained at the ground unit, tracking the sonde using triangulation.

The radiosonde transmits the measured temperature and relative humidity at each pressure level. The altitudes of these levels are calculated using the hypsometric equation. The recorded parameters are then plotted in a *thermodynamic diagram*, see figure 4.1. Note that there are many variations of thermodynamic diagrams possible. The diagram in figure 4.1 shows the *liquid water potential temperature* at the vertical lines, and pressure at the horizontal lines.[1] Using this convention, the vertical lines are *saturated adiabates*. The real temperature is shown as the diagonal straight lines. Furthermore the *dry adiabates* are indicated as the dotted curved lines. These lines represent the change in temperature that a dry air parcel would undergo if moved up and down in the atmosphere and allowed to expand or become compressed (in a dry adiabatic process) because of the air pressure change in vertical direction. The dry adiabates converge to the saturated adiabates at some height. Finally *isohumes* or *saturation mixing ratio lines* are shown as dashed diagonal lines. These lines define the maximum amount of water vapor that could be held in the atmosphere (the saturation mixing ratio) for each combination of temperature and pressure. These lines can be used to determine whether a parcel is saturated or not. For a certain pressure, the combination with the air temperature yields the saturation mixing ratio, and with the dew point temperature it yields the actual mixing ratio.

The combination of the dewpoint temperature and the air temperature in a thermodynamic diagram reveals a wealth of meteorological information on, e.g., cloud formation, atmospheric stability, and inversion layers.

The wind direction and speed is plotted using the standard meteorological convention for showing winds. The feathers, or *barbs*, indicate the wind speed: a long barb is 10 knots,

[1] The potential temperature is the temperature an air parcel would have at a certain reference pressure level if the dry adiabatic temperature changes during vertical displacement would be removed (Stull, 1995). In other words, if an air parcel is moved vertically in a dry adiabatic way, the potential temperature does not change. The liquid water potential temperature describes the temperature of a fully saturated parcel, moved vertically along the saturated adiabat.

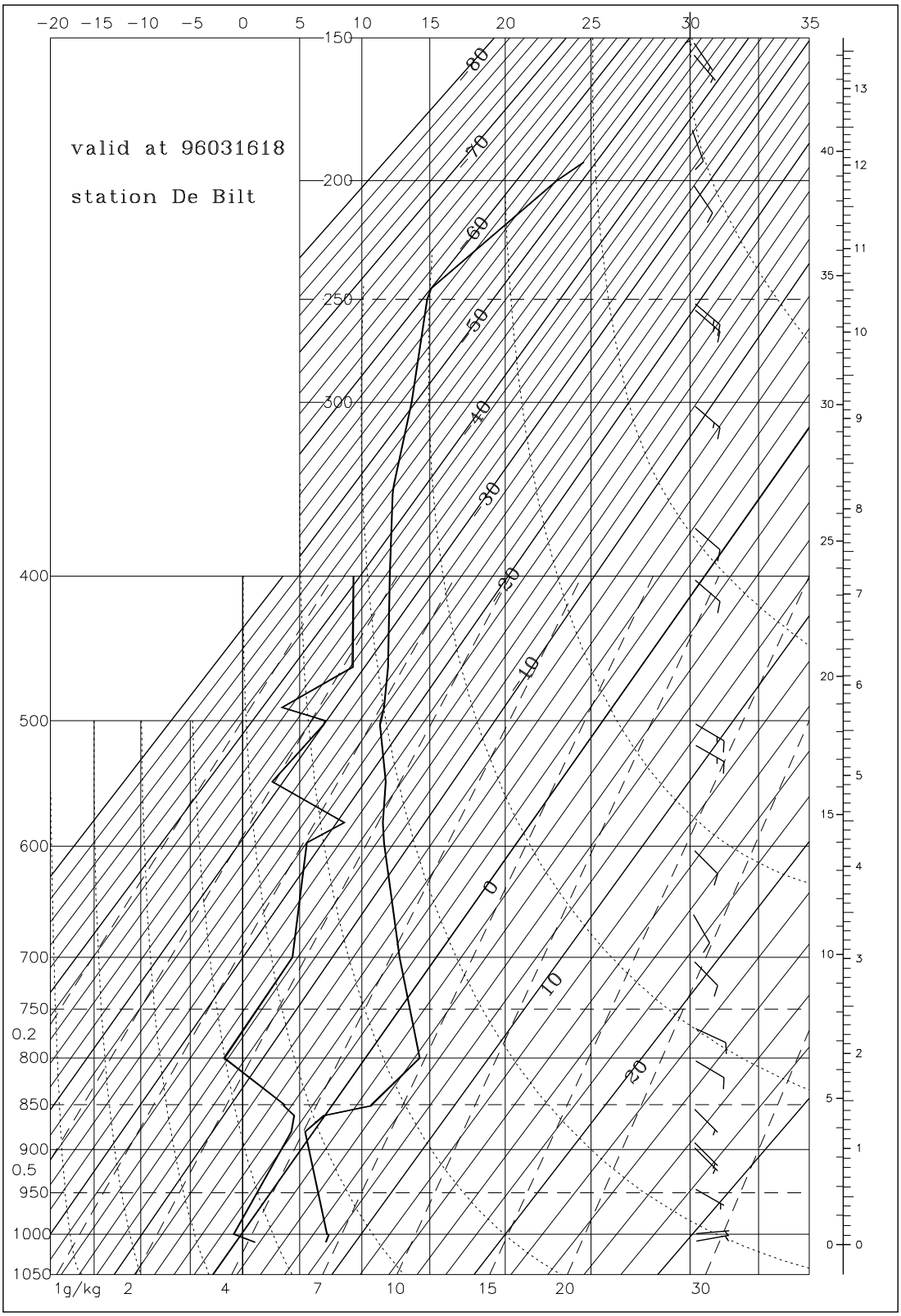

Figure 4.1 *Example of a radiosonde profile for De Bilt, 16 March 1996, 18:00 UTC , interferogram gd4*

or 5 m/s. A short barb is 5 knots or 2.5 m/s. The accuracy of the wind speeds is 2–3 m/s (ECMWF, 1994; Stull, 1995)

The radiosonde observations used for this study were obtained from the stations *De Bilt* in the Netherlands, *Ukkel* in Belgium, and *Emden* in Germany. The location of the stations is shown in figure 3.1. Two sondes, before and after each SAR acquisition, were used from the De Bilt station, and one sonde (the closest to the SAR acquisition) from the Emden and Ukkel stations. In total eight radiosonde profiles were analyzed for every interferogram.

4.2.4 Synoptic observations

Synoptic observations are obtained by a large number of manned or automatically operating meteorological stations. The different categories of observations are listed in table 4.2, and discussed below.

Code	Quantity	Units
stn	station number	
jjjjmmdd	Date	
uumm	Time (UTC)	h, m
t	Temperature	0.1°C
u	Relative humidity	%
rh	Amount of precipitation during the last hour	mm
dr	Duration if the precipitation in the last hour	0.1 h
dd	Average wind direction in the last 10 minutes of the last hour	degrees
ff	Average wind speed in the last 10 minutes of the last hour	0.1 m/s
q	Radiation during the last hour	J cm^{-2}
ww	Present weather category	code
v	Horizontal visibility	m
p	Pressure at sea level	mbar
n	Total cloud cover	octa
nh	Cloud cover low and medium clouds	octa
n1–n4	Cloud cover layer 1–4	octa
c1–c4	Cloud type or genus layer 1–4	code
h1–h4	Estimated height cloud base layer 1–4	code

Table 4.2 *Observation parameters at the synoptic stations*

Synoptic weather observations are stored in UTC and are available every whole hour. Airports often provide additional observations every half hour. The synoptic temperature `t` is determined at a height of 1.5 m above the ground level, with an accuracy of 0.1°C, and at the observation time. Relative humidity `u` is measured with an accuracy of a few percents. Precipitation, `rh`, in mm/hr is collected in the hour prior to reporting. Synoptic wind speeds `ff` and directions `dd` are measured at a height of 10 m above ground level. The reported wind speeds are mean values during 10 minutes of measurement. Wind speed accuracies are 3–4 m/s for surface stations (ECMWF, 1994; Stull, 1995). Table 4.3 lists the conversion between the Beaufort scale and its equivalent wind speed at a height of 10 m (McIlveen, 1995). The amount of solar radiation, `q`, can be interpreted as an

Beaufort	0	1	2	3	4	5	6	7	8	9	10	11
m/s	0	0.8	2.4	4.3	6.7	9.3	12.3	15.5	18.9	22.6	26.4	30.5

Table 4.3 *Conversion between the first 12 Beaufort wind forces and the equivalent mean wind speed at 10 m above the ground*

indirect measure of cloud cover. High radiation values mean that there is no cloud cover, low values imply thick cloud cover.

The weather code system—the `ww` observations in table 4.2—is a comprehensive range of codes to describe the particular behavior of the weather during the last hour or at observation time. It includes different degrees of haze and fog, development measures for clouds, types and patterns of precipitation, visibility measures, thunderstorm types, and different types of special weather phenomena. A list of weather codes can be found in, e.g., McIlveen (1995).

Pressure, `p`, is measured in mbar, currently often listed in hPa, and is measured with an accuracy of 0.1 mbar (ECMWF, 1994). Cloud cover, `n`, is defined as the fraction of the sky that is covered by clouds. It is estimated in fractions from 0/8 to 8/8, or *octa*, for the total cover and—if possible—for up to four height levels, `n1`–`n4`. The type of cloud cover, denoted by `c1`–`c4`, is a code for one of the 10 *genera*, see table 4.4, and is reported for every observed level of coverage. Furthermore, the height of each layer is estimated and reported, `h1`–`h4`.

Code	Genus	Level	Features
St	Stratus	Low	Low, spatially extensive sheet of cloud
Sc	Stratocumulus	Low	Low, broken into cumuliform masses
Cu	Cumulus	Low	Detached, hill shaped, flat base
Cb	Cumulonimbus	Low	Large cumulus, usually with showers. Large vertical extent
As	Altostratus	Medium	Extensive sheet, featureless
Ac	Altocumulus	Medium	Shallow sheet, broken into patches or rolls
Ns	Nimbostratus	Medium	Extensive sheet, usually precipitating
Ci	Cirrus	High	Detached, white fibrous clouds
Cc	Cirrocumulus	High	Shallow patch or sheet, broken into blobs or ripples
Cs	Cirrostratus	High	Shallow extensive sheet, transparent

Table 4.4 *Cloud classification in 10 genera, after McIlveen (1995). Low level clouds are at heights between 0–2 km above sea level, medium level at 2–7 km, and high level at 5–14 km, for temperate regions.*

The number of synoptic stations used in the analysis of the SAR interferograms vary according to the size of the interferogram area and the availability of the data. For all available stations, observations are used on the hours before and after each SAR acquisition. Cloud observations and weather codes are only available at the manned meteorological stations, mostly at airfields. These are listed in the interferogram analyses in chapter 5.

Based on the wind direction and velocity measured at the stations, interpolated surface wind fields are plotted to enable a comparison with the interferograms. Furthermore interpolated pressure and temperature fields are calculated. If these plots significantly enhance the interpretation of a specific interferogram, they are included in the analysis in chapter 5.

4.2.5 Weather charts

Weather charts, as provided by national and international meteorological services, are a combination of observations from different sensors and their meteorological situation. The weather charts used in this study are daily overviews of the weather over Europe at 12:00 UTC. They mainly show the location of high and low pressure regions and the isobars. Frontal systems are drawn over this plot. Selected surface observations of the main synoptic stations in the region are included, giving information on the temperature, wind speed and direction, total cloud cover, and precipitation. Five selected stations in the Netherlands are listed, with average values for the whole day for windspeed, temperature at two height levels, water vapor pressure, relative humidity, and pressure. Furthermore total values for the amount and duration of precipitation, and the duration of sunshine during the day. Although the information obtained from these charts is limited, it can give a rough estimation on the type and dynamics of the weather during that day. The plots are not shown during the interpretation of the interferograms in chapter 5 for the sake of conciseness.

4.3 Meteorological models

Weather analysis is the operational procedure for characterizing the spatial structure of the atmosphere at a specific time or epoch (Bevis et al., 1996). Initial state analyses are produced twice daily by most operational analysis centers, and are assimilated in a numerical weather model to produce weather forecasts. In Europe, the ECMWF[2] applies a model with a horizontal resolution of about 60 km, and 31 vertical layers. Meteorological variables are computed every 15 minutes (Stull, 1995). In the Netherlands the HIgh Resolution Limited Area Model (HIRLAM) is used. Resolutions are 55 to 5 km horizontally with 16 to 31 vertical layers. The Netherlands' implementation of the HIRLAM model applies a 3-hourly variational data assimilation scheme, using a cut-off time of 2h50 after the initialization time. The boundary values for the HIRLAM domain are taken from the ECMWF model output.

Since the model data described above lack in spatial resolution for the purpose of SAR interferometry, they were not used in the interferogram analyses. The specific disturbances in the interferograms are often of a smaller spatial extent. Moreover, these types of disturbances mostly apply on smaller time scales than the 3 hour averages in a model such as HIRLAM.

Just as the daily weather charts, model data can be used to get an overview of the meteorological conditions during the SAR acquisitions. This enables one to get likelihood estimates for specific types of disturbance. The readily availability of model data makes this type of information convenient for the analysis of larger regions, e.g., to select suitable

[2]European Center for Medium-Range Weather Forecasts

interferometric pairs from a database of SAR imagery.

4.4 Meteorological codes

Meteorological codes are used to facilitate quick information exchange with a format which enables automatic data processing. They are defined by the World Meteorological Organization in WMO Manual No. 306. The codes are composed of a set of code forms and binary codes made up of groups of letters representing meteorological or other geophysical elements. Different code forms are used to represent different types of observations or products. In messages, these groups of letters are transcribed into figures indicating the value of state of the elements described (Darling and Mongeon, 1996).

Chapter 5

Analysis and interpretation

Here, the set of interferograms is analyzed using all available meteorological information. It first describes the used methodology, and lists the main characteristics of the interferograms. Hereafter, the interferograms are analyzed by observing the possible atmospheric effects, interpreting these observations using suitable meteorological information, and providing concluding remarks per situation. The chapter concludes with a discussion of the analyses, in which the results are merged and classified.
key words: methodology, analysis, interpretation, classification

5.1 Analysis techniques

Although each computed interferogram should in fact be analyzed in a way optimized for the particular situation, a more or less standardized approach was chosen here to facilitate overall comparison and conclusions on the magnitude and type of recurrent effects. This results in a specific setting for each interferogram. Nevertheless, when phenomena are observed who deserve any special attention, also different analysis techniques were applied.

The interferograms are categorized according to their location into four groups: Groningen descending, Flevoland ascending, Flevoland descending, and Delft descending. Within each group, the interferograms are ordered chronologically. After a brief summary of the technical characteristics of the interferogram, three subsections list the specific interferometric *observations*, the *interpretation* of the observations using meteorological information, and the *conclusions* on the atmospheric signatures in the interferogram.

For every interferogram the relative and absolute phase are shown in the observation section, corresponding with the wrapped and unwrapped interferograms. The original, wrapped, interferogram has a phase fixed between $-\pi$ and $+\pi$, which enables a quick impression of the complexity of the phase variations. The phase scale of the unwrapped interferogram increases with the number of fringes, and is unique for every interferogram. If necessary, phase variations induced by topography are extracted using a reference DEM, which produces the differential interferogram. For the areas with few topography, combined with small perpendicular baselines, the original interferogram can be regarded as a differential interferogram. It is assumed that the only remaining interferometric phase variations are caused by horizontal spatial variations in the path delay.

A statistical analysis of the phase is then performed using a histogram, which also yields a rms value. There are two important consequences of this approach. First, obviously,

the phase can only be analyzed over sufficiently coherent areas, e.g., excluding the water parts formed by the North Sea and IJsselmeer. Therefore, if necessary, in the histogram analysis several patches were selected who jointly contribute to the histogram. Since every patch has its own distribution, with a mean which can be different from other patches, the total histogram is sometimes composed of more than one more or less Gaussian distribution. Secondly, because the total surface of the selected patches is different for every interferogram, it is hard to use, e.g., the derived rms value as representative for the atmospheric phase variation. The combined interferograms of the Flevoland-ascending passes will therefore have larger rms values than the single-interferograms of Groningen. However, it is tried to use the same area of analysis per location, and therefore the results per location are comparable.

The standard observations conclude with the plot of a rotationally averaged spectrum of the largest possible rectangle in the interferogram. Plotting this spectrum on a log-log scale enables the comparison of the spectral frequencies with the $-5/3$ power law lines, commonly associated with turbulence in Kolmogorov theory. For the theoretical background of this evaluation, see section 2.4.5. The plots are shown to test the method to identify turbulent regions, and to discriminate different types of atmospheric signature in the SAR interferograms.

Following the observations, the data for each interferogram are interpreted, using all information available. The meteorological data sources are described in section 4.2. Since the amount of data used for each interpretation is too large to be fully printed in this report, only some derived and condensed plots, tables, or graphs are shown in the interpretations. For some of the interferograms, first hypotheses are given at the start of the interpretation, based on the interferogram only, or in combination with the daily weather charts.

Finally, conclusions are derived for every interferometric situation. The most probable cause or hypothesis for the observed differential phase variation is described, based on the available information. Some statistical information is summarized.